Mon. Not. R. Astron. Soc. **348,** 1175–1190 (2004) doi:10.1111/j.1365-2966.2004.07420.x

Magnetic topology and surface differential rotation on the K1 subgiant of the RS CVn system HR 1099

P. Petit,[1,2⋆] J.-F. Donati,[1⋆] G. A. Wade,[3⋆] J. D. Landstreet,[4⋆] S. Bagnulo,[5⋆] T. Lüftinger,[6⋆] T. A. A. Sigut,[4⋆] S. L. S. Shorlin,[4⋆] S. Strasser,[7⋆] M. Aurière[1⋆] and J. M. Oliveira[8⋆]

[1]*Laboratoire d'Astrophysique, Observatoire Midi-Pyrénées, 14 Av. E. Belin, F–31400 Toulouse, France*
[2]*Centro de Astrofisica da Universidade do Porto, rua das Estrelas, 4150-762 Porto, Portugal*
[3]*Royal Military College of Canada, Department of Physics, PO Box 17000, Station "Forces", Kingston, Ontario K7K 4B4, Canada*
[4]*Department of Physics and Astronomy, The University of Western Ontario, London, Ontario N6G 3K7, Canada*
[5]*European Southern Observatory, Alonso de Cordova 3107, Vitacura, Santiago, Chile*
[6]*Institut für Astronomie, Tuerkenschanzstrasse 17, A-1180 Wien, Austria*
[7]*Department of Physics and Astronomy, University of Calgary, Calgary, AB T2N 1N4, Canada*
[8]*Department of Physics, Keele University, Staffordshire ST5 5BG*

Accepted 2003 November 12. Received 2003 September 26; in original form 2003 January 9

ABSTRACT

We present here spectropolarimetric observations of the RS CVn system HR 1099 (V711 Tau) secured from 1998 February to 2002 January with the spectropolarimeter MuSiCoS at the Télescope Bernard Lyot (Observatoire du Pic du Midi, France). We apply Zeeman–Doppler imaging and reconstruct surface brightness and magnetic topologies of the K1 primary subgiant of the system, at five different epochs. We confirm the presence of large, axisymmetric regions where the magnetic field is mainly azimuthal, providing further support to the hypothesis that dynamo processes may be distributed throughout the whole convective zone in this star.

We study the short-term evolution of surface structures from a comparison of our images with observations secured at close-by epochs by Donati et al. at the Anglo-Australian Telescope. We conclude that the small-scale brightness and magnetic patterns undergo major changes within a time-scale of 4–6 weeks, while the largest structures remain stable over several years.

We report the detection of a weak surface differential rotation (both from brightness and magnetic tracers) indicating that the equator rotates faster than the pole with a difference in rotation rate between the pole and the equator about four times smaller than that of the Sun. This result suggests that tidal forces also affect the global dynamic equilibrium of convective zones in cool active stars.

Key words: polarization – stars: activity – binaries: close – stars: imaging – stars: magnetic fields – stars: rotation.

1 INTRODUCTION

In classical solar dynamo theories, differential rotation plays a key role in the generation of the solar magnetic field, through its ability to transform a poloidal field into a stronger toroidal component. This so-called 'Ω effect' is thought to take place in a thin layer at the interface between the radiative core and the convective envelope of the Sun (the tachocline). A poloidal component of the field is then regenerated by cyclonic convection (with opposite polarity), therefore producing what is known as the solar magnetic activity cycle.

Dynamo processes generating magnetic activity on stars other than the Sun can now be directly investigated through images of their photospheric brightness and magnetic topologies, thanks to the development of Zeeman–Doppler imaging (hereafter ZDI, Donati & Brown 1997). The long-term monitoring of a sample of active fast rotators shows that they all possess regions of strong, nearly

⋆E-mail: petit@astro.up.pt (PP); donati@ast.obs-mip.fr (JFD); auriere@ast.obs-mip.fr (MA); Gregg.Wade@rmc.ca (GAW); jlandstr@astro.uwo.ca (JDL); asigut@astro.uwo.ca (TAAS); sshorlin@astro.uwo.ca (SLSS); sbagnulo@eso.org (SB); theresa@tycho.astro.univie.ac.at (TL); strasser@ras.ucalgary.ca (SS); joana@astro.keele.ac.uk (JMO)

azimuthal magnetic field, features that are not expected to show up at photospheric level in the context of the conventional solar dynamo. Such observations suggest that the Ω effect is not confined in the tachocline of these objects, but may be instead distributed throughout their convective envelope, and at least be efficient close to the photosphere.

In addition to yielding information about the magnetic topology, indirect imaging techniques provide the first opportunity for monitoring the short-term evolution of brightness and magnetic inhomogeneities at the surface of active stars, under the influence of differential rotation. The first results, derived from observations of several young fast rotators (Donati & Cameron 1997; Donati et al. 1999a, 2000; Barnes et al. 2000; Cameron, Donati & Semel 2002; Donati, Cameron & Petit 2003b) show that their surface rotational shear is of the same magnitude as that of the Sun, with a trend to increase toward higher stellar masses (as confirmed by the observations of Reiners & Schmitt 2002 on a sample of F-type fast rotators).

The K1 primary subgiant of the RS CVn system HR 1099 is one of the most active stars in the whole sky. The complex surface magnetic field of this object has already been mapped by Donati et al. (1992), Donati (1999) and Donati et al. (2003a), confirming that efficient dynamo processes are operating within its deep convective envelope. Unfortunately, the first attempts at estimating differential rotation at the surface of this object (Vogt et al. 1999; Strassmeier & Bartus 2000) were not convincing because they were based on data of relatively low signal-to-noise ratio (S/N) and sparse phase sampling (Petit, Donati & Cameron 2002). However, a rigorous analysis of the surface differential rotation of this star should provide useful information complementary to magnetic imaging, for investigating the dynamo mechanisms driving its impressive activity. Finally, the present study is of special interest as it concerns a star with different evolutionary status than those studied to date, featuring in particular a very deep convective zone and subject to intense tidal forces.

In the present paper, we report new spectropolarimetric observations of HR 1099 secured between 1998 and 2002 at Observatoire du Pic du Midi (France), from which we reconstruct brightness and magnetic images of its primary subgiant by means of ZDI. Comparisons are made with observations of the same object secured by Donati et al. (2003a) (D03a from now on) at the Anglo-Australian Telescope (AAT) a few weeks apart from, and sometimes simultaneously with, our own observations. We take the original opportunity of comparing images obtained with different instrumental set-ups and observing conditions for providing further testing of the robustness of ZDI. We also study the short-term evolution of surface structures by comparison with observations of D03a obtained within a few weeks of our own data.

We then apply the method of Petit et al. (2002) to estimate the surface rotational shear from brightness and magnetic images. We compare our results with the work of Donati, Cameron & Petit (2003b) (hereafter D03b), who derived a first estimate of differential rotation on this star using the same method, but from data sets substantially smaller than ours. We also discuss the possibility of detecting temporal fluctuations of the shear, as reported by D03b for younger objects.

We finally summarize the results and investigate the possible connection of the measured surface shear with the observed lifetime of surface structures, as well as the possible impact of tidal forces on the differential rotation of HR 1099.

2 OBSERVATIONS AND DATA PREPARATION

2.1 Data collection and reduction

The polarized spectral data used in this paper were secured with Télescope Bernard Lyot (TBL) at Observatoire du Pic du Midi (France) between 1998 February and 2002 January, using the MuSiCoS echelle spectrograph (Baudrand & Böhm 1992) fibre fed from a Cassegrain-mounted polarimetric module (Donati et al. 1999a). The data reduction was performed with ESPRIT, following the procedure developed by Donati et al. (1997).

The journal of observations is reported in Tables 1–4. We divide the observations into five separate groups, corresponding to different observing periods (epoch 1998.14 in Table 1, epochs 1998.93 and 1999.06 in Table 2, epoch 2000.14 in Table 3 and epoch 2001.96 in Table 4). This observing effort yielded a total of 104 polarized exposures secured over 72 telescope nights. Exposures in circular polarization (Stokes V) consist of a sequence of four subexposures taken with the quarter-wave plate oriented at azimuth $\pm 45^\circ$ with respect to the optical axis of the beam-splitter. Each of these individual subexposures is used to produce an intensity spectrum (Stokes I), thus allowing us to take advantage of the finer phase resolution (of the order of 1.5×10^{-3} rotation cycle for an exposure of 360 s) between successive subexposures. The total number of Stokes I spectra reported in this study is 420.

Least-square deconvolution (LSD, Donati et al. 1997) is employed to extract simultaneously the information from most spectral lines available in the observed wavelength domain. The spectral line list used to produce the LSD profiles of HR 1099 corresponds to the same K1 photospheric mask as that employed in Donati (1999). A total of about 2600 spectral features are taken into account for the present data sets as opposed to about 4500 in the study of D03a. This difference results from the smaller spectral range of MuSiCoS (450 to 660 nm in polarimetric mode), which reduces the number of spectral lines available for LSD. The resulting Stokes V profiles benefit from a multiplex gain of about 30 (see Tables 1–4) as opposed to an average multiplex gain of 40 for AAT profiles. Most Stokes I LSD profile S/N values stay between 900 and 1000, following the behaviour pointed out by Donati et al. (1997), and indicating that the convolution model underlying LSD cannot be trusted above this level of accuracy.

The wavelength calibration, automatically performed by ESPRIT with reference to a thorium–argon spectrum, has been refined for the present study by means of a new procedure involving telluric lines, and is similar to that described in D03a. This method consists in running LSD on each stellar spectrum with a special mask including telluric lines only. The measured shift of the derived LSD telluric profiles from a null velocity (in the terrestrial frame) is attributed to instrumental instability and used to correct the wavelength scale. This method permits an exposure-by-exposure calibration, thus suppressing the instrumental drifts occurring throughout the nights. The accuracy of the telluric line calibration (which can roughly be evaluated, for example, by the average wavelength shift between two successive exposures) is of order 300 m s^{-1}, which is not as good a value as that reached with UCLES at the AAT ($<$100 m s^{-1}). Most of the difference can be attributed to the smaller spectral range of TBL (especially in the red region), which reduces the number of telluric lines available, as well as to the site quality of Observatoire du Pic du Midi (where the telluric spectrum is usually weak, thanks to the altitude of the telescope). Applying this technique shows that the wavelength shift across the night can be either slow and

Table 1. Journal of observations for epoch 1998.14. Each line corresponds to a full polarization cycle. The two figures separated by a '/' give the minimum and maximum value of each field, except in column 4, which lists the number of unpolarized/polarized spectra. Column 5 lists the total exposure time of each Stokes I individual subexposure. We also list the S/N ratios (per 4 km s^{-1} velocity bins) of the unpolarized and polarized spectra (in columns 6 and 8 respectively) and in the associated mean LSD profiles (columns 7 and 9). The multiplex gain between the raw polarized spectra and the mean Stokes V profiles is reported in the last column.

Date	JD (+245 0000)	UT (hh:mm:ss)	nexp	$t_{\rm exp}$ (s)	S/N I	S/N $I_{\rm LSD}$	S/N V	S/N $V_{\rm LSD}$	Multiplex gain V
1998 Feb 4	849.317/849.332	19:35:43/19:58:22	4/1	360	160/170	864/873	330	12020	36
1998 Feb 5	850.311/850.335	19:27:27/20:01:50	5/1	360	130/140	958/964	270	9081	33
1998 Feb 6	851.307/851.323	19:22:30/19:45:22	4/1	360	140/150	957/960	290	9719	33
1998 Feb 7	852.296/852.328	19:06:00/19:53:00	5/1	600	130/150	939/956	310	10133	32
1998 Feb 8	853.324/853.340	19:46:48/20:09:00	4/1	360	110/140	827/844	250	8023	32
1998 Feb 9	854.345/854.363	20:16:49/20:43:26	4/1	360	160/170	958/965	330	10516	31
1998 Feb 10	855.377/855.394	21:03:00/21:26:45	4/1	360	140/150	984/993	300	9523	31
1998 Feb 11	856.341/856.357	20:11:03/20:33:36	4/1	360	160/170	845/848	330	11178	33
1998 Feb 12	857.301/857.317	19:13:35/19:35:43	4/1	360	160/180	954/958	350	11989	34
1998 Feb 13	858.316/858.337	19:35:11/20:05:00	5/1	360	150/170	981/985	360	12351	34
1998 Feb 14	859.326/859.339	19:49:11/20:07:34	4/1	300	110/120	884/893	230	7101	30
1998 Feb 15	860.337/860.351	20:05:35/20:26:02	4/1	300	87/90	908/915	170	4781	28
1998 Feb 16	861.339/861.353	20:08:33/20:28:09	4/1	300	110/120	978/982	240	8275	34
1998 Feb 17	862.310/862.323	19:26:04/19:45:27	4/1	300	100/110	910/927	210	6505	30
1998 Feb 18	863.291/863.307	18:59:25/19:21:42	4/1	360	120/140	900/910	250	7986	31
1998 Feb 20	865.319/865.342	19:39:32/20:13:05	4/1	600	92/120	937/949	210	6600	31
1998 Feb 26	871.353/871.369	20:28:14/20:50:56	4/1	360	100/110	937/954	200	5657	28
1998 Feb 27	872.328/872.343	19:51:50/20:14:20	4/1	360	140/140	898/907	280	8536	30
1998 Feb 28	873.359/873.375	20:36:40/20:59:23	4/1	360	120/150	842/845	270	7715	28
1998 Mar 2	875.348/875.364	20:20:50/20:44:10	4/1	360	100/120	940/964	220	6189	28
1998 Mar 5	878.377/878.394	21:02:58/21:27:29	4/1	360	95/100	528/931	190	3514	18

Table 2. Same as Table 1 for epochs 1998.93 and 1999.06.

Date	JD (+245 0000)	UT (hh:mm:ss)	nexp	$t_{\rm exp}$ (s)	S/N I	S/N $I_{\rm LSD}$	S/N V	S/N $V_{\rm LSD}$	Multiplex gain V
1998 Dec 5	1153.3298/1153.3528	19:54:56/20:27:58	4/1	360	96/102	930/977	195	5912	30
1998 Dec 5	1153.4280/1153.4445	22:16:22/22:40:04	4/1	360	95/122	978/979	230	7458	32
1998 Dec 6	1153.5307/1153.5492	00:44:15/01:10:50	4/1	420	127/154	973/987	275	8792	32
1998 Dec 6	1153.6077/1153.6237	02:35:03/02:58:11	4/1	360	68/88	923/964	159	4396	28
1998 Dec 7	1155.4395/1155.4554	22:32:49/22:55:44	4/1	360	92/125	854/932	224	7036	31
1998 Dec 8	1155.5910/1155.6070	02:11:04/02:34:09	4/1	360	97/112	836/864	206	5543	27
1998 Dec 8	1156.3413/1156.3572	20:11:27/20:34:22	4/1	360	47/60	822/862	106	2981	28
1999 Jan 13	1192.2812/1192.2958	18:44:54/19:06:00	4/1	360	103/127	878/909	226	6885	30
1999 Jan 14	1193.3795/1193.3943	21:06:26/21:27:46	4/1	360	105/127	942/954	232	7152	31
1999 Jan 19	1198.3154/1198.3303	19:34:10/19:55:34	4/1	360	131/148	827/840	280	9278	33
1999 Jan 22	1201.3794/1201.3942	21:06:21/21:27:38	4/1	360	142/148	933/944	284	8837	31
1999 Jan 23	1202.3167/1202.3315	19:36:07/19:57:22	4/1	360	165/178	893/921	344	11339	34
1999 Jan 24	1203.3362/1203.3557	20:04:00/20:32:11	4/1	360	116/125	898/907	238	7347	31
1999 Jan 25	1204.3249/1204.3399	19:47:48/20:09:24	4/1	360	99/110	906/942	205	6306	31
1999 Jan 30	1209.3488/1209.3634	20:22:20/20:43:20	4/1	360	45/48	540/602	93	2504	27
1999 Jan 31	1210.2966/1210.3114	19:07:10/19:28:22	4/1	360	93/108	833/897	198	5995	30
1999 Jan 31	1210.3627/1210.3814	20:42:14/21:09:10	4/1	480	116/128	890/915	242	7486	31

progressive or abrupt and very fast (i.e. between two successive exposures separated by a few minutes), reaching as much as 2 km s^{-1}, i.e. more than six times the accuracy of the telluric line calibration. We thus conclude that such wavelength calibration is significantly better than that achieved from thorium–argon spectra alone.

2.2 Imaging procedure

All the brightness and magnetic images described in this paper are obtained with the imaging code developed by Brown et al. (1991) and Donati & Brown (1997), following the principles of maximum-entropy image reconstruction outlined by Skilling & Bryan (1984). The behaviour of this imaging procedure was tested for various stellar parameters and observing conditions by Donati & Brown (1997), from a series of numerical simulations. They demonstrated that regions in which the field orientation is azimuthal can clearly be distinguished from radial or meridional field structures (for noise levels similar to that available for the present study). Some of their conclusions should, however, be kept in mind in the specific case of HR 1099, as outlined by Donati (1999). In particular, we expect partial cross-talk between radial and meridional field components located at low latitudes, owing to the relatively low inclination angle

Table 3. Same as Table 1 for epoch 2000.14.

Date	JD (+245 0000)	UT (hh:mm:ss)	Nexp	t_{exp} (s)	S/N I	S/N I_{LSD}	S/N V	S/N V_{LSD}	Multiplex gain V
2000 Feb 3	1578.3474/1578.3738	20:20:15/20:58:15	6/1	360	83/97	861/877	170	5062	29
2000 Feb 4	1579.3538/1579.3688	20:29:24/20:51:01	4/1	360	66/76	882/915	130	4251	32
2000 Feb 5	1580.3578/1580.3779	20:35:16/21:04:00	4/1	360	38/67	534/773	230	6618	28
2000 Feb 9	1584.3295/1584.3441	19:54:30/20:15:30	4/1	360	110/130	917/932	100	2326	23
2000 Feb 11	1586.3744/1586.3890	20:59:10/21:20:10	4/1	360	98/100	920/956	200	5089	25
2000 Feb 12	1587.3340/1587.3486	20:00:56/20:21:56	4/1	360	130/140	971/991	270	8069	29
2000 Feb 15	1590.3453/1590.3599	20:17:10/20:38:13	4/1	360	100/110	982/994	210	5812	27
2000 Feb 22	1597.3141/1597.3290	19:32:21/19:53:43	4/1	360	140/150	975/980	280	8352	29
2000 Feb 24	1599.3157/1599.3303	19:34:37/19:55:39	4/1	360	110/120	994/1007	220	6015	27
2000 Feb 25	1600.3060/1600.3206	19:20:40/19:41:37	4/1	360	130/150	975/987	270	8213	30
2000 Feb 26	1601.3236/1601.3383	19:45:56/20:07:00	4/1	360	130/100	893/904	220	6249	28
2000 Feb 27	1602.3092/1602.3241	19:25:17/19:46:40	4/1	360	100/120	969/983	220	6434	29
2000 Mar 2	1606.3150/1606.3301	19:33:32/19:55:24	4/1	360	120/140	992/1007	270	7530	27
2000 Mar 3	1607.3187/1607.3345	19:38:57/20:01:39	3/0	600	49/60	618/761	–	–	–
2000 Mar 4	1608.2950/1608.3100	19:04:50/19:26:26	4/1	360	140/150	872/879	290	8249	28
2000 Mar 5	1609.2978/1609.3125	19:08:53/19:30:04	4/1	360	92/100	769/865	180	5059	28
2000 Mar 8	1612.2965/1612.3113	19:06:57/19:28:17	4/1	360	110/130	798/948	230	7319	31

of the star. Moreover, in case of images computed with incomplete phase sampling, only a partial reconstruction of the magnetic field is achieved, containing radial/meridional field regions closest to the observed longitudes and azimuthal field structures located about 0.2 rotation cycle away from the observed longitudes.

To model the photospheric brightness inhomogeneities, we use the two-component description of Cameron (1992), in which every pixel of the stellar surface includes a fraction f of quiet photosphere (of temperature 4750 K) and $1 - f$ of cool spot (of temperature 3500 K). The average intrinsic profile used for modelling the observed LSD spectra and computing brightness images is a synthetic Gaussian line reproducing the characteristics of a MuSiCoS LSD Stokes I profile of the K0 star β Gem. This option was adopted according to the results of Unruh & Cameron (1995), who demonstrated that Doppler images reconstructed from a Gaussian line were almost indistinguishable from that obtained using a standard star. The use of a synthetic line further guarantees that the template is free from noise. This Gaussian profile was scaled by a factor 0.5 and 1 for the spotted areas and the quiet photosphere, respectively, as suggested by the observations of Donati & Cameron (1997).

Before reconstructing brightness and magnetic images of the primary component of HR 1099, one must first perform a careful removal of the contribution from the G5 secondary component to the system spectra, following the method outlined by Donati et al. (1992). This correction consists in suppressing the line of the secondary star (assumed Gaussian) in every Stokes I profile of the system at conjunction phases. We assume that the contribution of the secondary star can be neglected in Stokes V profiles, as discussed by Donati (1999). Then one has to correct for the orbital motion of the primary star. Both operations require a precise estimate of the system orbital parameters.

The radial velocity amplitude K_s of the secondary star, the radial mean velocity shift γ of the system and the phase of conjunction ϕ_0 of both stars are listed in Table 5. These values are in very good agreement with estimates derived from AAT data at close-by epochs. We thus confirm the stability of K_s and γ over years, and the persistent decrease of ϕ_0, by an average of 0.89 per cent of a rotation cycle in one year. The determination of the velocity amplitude $v \sin i$ and inclination i of the primary star is discussed by Donati (1999). In this paper, we set these parameters to 40 Km s^{-1} and 38° respectively (slightly different from, though still compatible with, Donati 1999), to provide the best fit to our data.

3 RECONSTRUCTED IMAGES

The five brightness and magnetic images obtained for the different observing epochs are described in this section. In order to allow easy comparisons (and keep consistent) with previous work presenting ZDI images of HR 1099 (Donati 1999 D03a), the reconstructed magnetic field is divided into its three components in spherical coordinates, each one being displayed in a grey-scale chart. In recent studies, some authors prefer to display 3D field lines in one single chart (see, e.g. Piskunov 2001), with the obvious advantage that the field orientation is therefore directly seen on the map. This second option may be well-adapted to the case of chemically peculiar stars, hosting a large-scale field varying smoothly over the stellar photosphere. On the surface of cool active stars, however, individual magnetic regions cover only a small fraction of the photosphere and the orientation of field lines can vary a lot from one region to the other. In this specific case, 3D field lines would therefore produce a tangled pattern, very hard (if not impossible) to interpret. Displaying three distinct maps appears to be a good compromise in this context, but the reader should keep in mind that the exact orientation of field lines inside active regions can only be deduced from a comparison of all three subcomponents of the magnetic field.

3.1 Phase sampling and time-span of observations

Three of the data sets studied in this paper present a time-span of observations of order one month (30 nights at epoch 1998.14, 35 nights for 2000.14 and 37 nights for 2001.96). The rather substantial number of Stokes I and V profiles constituting these data sets (200 Stokes I/50 Stokes V profiles for epoch 2001.96, 65/15 for 2000.14, 87/21 for 1998.14, see Tables 4, 3 and 1) provides a very dense (and sometimes even redundant) phase coverage (for epochs 1998.93 and 1999.06, large phase gaps only allow a partial reconstruction of the brightness and magnetic topologies). However, the drawback of this long time interval of data collection is that the images we present are

Table 4. Same as Table 1 for epoch 2001.96.

Date	JD (+245 0000)	UT (hh:mm:ss)	Nexp	t_{exp} (s)	S/N I	S/N I_{LSD}	S/N V	S/N V_{LSD}	Multiplex gain V
2001 Dec 1	2245.4601/2245.4756	23:02:32/23:24:53	4/1	400	119/142	888/890	265	8428	31
2001 Dec 2	2245.5809/2245.5964	01:56:32/02:18:53	4/1	400	117/124	908/917	243	7125	29
2001 Dec 2	2246.3264/2246.3419	19:49:59/20:12:21	4/1	400	106/114	942/956	217	6589	30
2001 Dec 2	2246.4399/2246.4554	22:33:29/22:55:50	4/1	400	106/156	948/960	260	8160	31
2001 Dec 3	2246.5517/2246.5673	01:14:30/01:36:52	4/1	400	142/157	913/924	303	9354	30
2001 Dec 5	2249.3259/2249.3415	19:49:22/20:11:43	4/1	400	63/86	869/906	148	4301	28
2001 Dec 5	2249.4378/2249.4533	22:30:24/22:52:46	4/1	400	69/95	692/792	158	4622	29
2001 Dec 6	2249.5052/2249.5207	00:07:25/00:29:46	4/1	400	52/64	519/612	112	3092	27
2001 Dec 6	2250.3536/2250.3692	20:29:15/20:51:36	4/1	400	110/115	909/924	251	7893	31
2001 Dec 6	2250.4447/2250.4603	22:40:26/23:02:48	4/1	400	121/124	919/944	215	5498	25
2001 Dec 7	2250.5738/2250.5894	01:46:18/02:08:40	4/1	400	117/123	915/930	222	6776	30
2001 Dec 7	2251.3256/2251.3411	19:48:52/20:11:13	4/1	400	124/136	936/951	244	7658	31
2001 Dec 7	2251.4368/2251.4524	22:29:02/22:51:24	4/1	400	124/130	941/954	236	6713	28
2001 Dec 8	2251.5824/2251.5979	01:58:39/02:21:01	4/1	400	105/108	918/947	279	8972	32
2001 Dec 8	2252.3268/2252.3423	19:50:34/20:12:55	4/1	400	123/127	860/869	281	8961	31
2001 Dec 8	2252.4595/2252.4750	23:01:37/23:23:58	4/1	400	110/124	828/846	282	7662	27
2001 Dec 9	2252.5721/2252.5876	01:43:49/02:06:11	4/1	400	115/117	877/888	260	8243	31
2001 Dec 9	2253.4321/2253.4476	22:22:10/22:44:31	4/1	400	124/127	949/958	252	7928	31
2001 Dec 10	2253.5768/2253.5923	01:50:38/02:12:59	4/1	400	111/118	928/932	212	5772	27
2001 Dec 10	2254.3562/2254.3717	20:32:55/20:55:16	4/1	400	130/137	975/984	248	7833	31
2001 Dec 10	2254.4663/2254.4818	23:11:28/23:33:49	4/1	400	128/131	972/980	231	7159	30
2001 Dec 11	2254.5791/2254.5946	01:53:52/02:16:13	4/1	400	124/131	964/979	232	6487	27
2001 Dec 11	2255.3328/2255.3483	19:59:12/20:21:34	4/1	400	119/131	846/857	249	7869	31
2001 Dec 11	2255.4660/2255.4815	23:10:59/23:33:21	4/1	400	109/131	901/919	231	6324	27
2001 Dec 12	2255.5897/2255.6052	02:09:00/02:31:28	4/1	400	78/102	875/921	268	8339	31
2001 Dec 12	2256.3289/2256.3445	19:53:40/20:16:02	4/1	400	134/144	945/949	259	8183	31
2001 Dec 12	2256.4443/2256.4599	22:39:51/23:02:12	4/1	400	148/155	919/934	251	7000	27
2001 Dec 13	2256.5549/2256.5704	01:19:00/01:41:21	4/1	400	132/136	881/891	250	7747	30
2001 Dec 13	2257.3309/2257.3465	19:56:34/20:18:55	4/1	400	195/200	825/878	236	7361	31
2001 Dec 13	2257.4459/2257.4614	22:42:03/23:04:25	4/1	400	187/190	733/834	180	4916	27
2001 Dec 14	2257.5264/2257.5419	00:37:59/01:00:20	4/1	400	174/176	696/751	276	8494	30
2001 Dec 16	2259.5505/2259.5661	01:12:46/01:35:08	4/1	400	61/78	816/842	303	9797	32
2001 Dec 16	2260.3293/2260.3448	19:54:10/20:16:31	4/1	400	152/159	972/978	270	7972	29
2001 Dec 16	2260.4268/2260.4423	22:14:36/22:36:58	4/1	400	126/159	947/967	291	9142	31
2001 Dec 17	2260.5529/2260.5684	01:16:11/01:38:33	4/1	400	123/127	896/937	261	8311	31
2001 Dec 17	2261.2953/2261.3108	19:05:13/19:27:36	4/1	400	134/146	939/954	185	5425	29
2001 Dec 17	2261.4359/2261.4515	22:27:46/22:50:09	4/1	400	144/146	932/948	140	3731	26
2001 Dec 18	2261.5424/2261.5580	01:01:00/01:23:27	4/1	400	131/141	914/938	310	10226	32
2001 Dec 18	2262.2848/2262.3004	18:50:08/19:12:31	4/1	400	134/154	856/858	294	9494	32
2001 Dec 18	2262.4283/2262.4438	22:16:42/22:39:05	4/1	400	120/157	845/852	249	7105	28
2001 Dec 19	2262.5537/2262.5692	01:17:19/01:39:41	4/1	400	115/128	823/862	280	8646	30
2001 Dec 20	2264.2891/2264.3046	18:56:17/19:18:40	4/1	400	94/105	917/930	289	9152	31
2001 Dec 21	2265.2786/2265.2941	18:41:07/19:03:30	4/1	400	88/135	858/877	274	7798	28
2001 Dec 22	2266.2873/2266.3028	18:53:43/19:16:06	4/1	400	97/103	924/939	291	9180	31
2001 Dec 27	2271.4947/2271.5169	23:52:26/00:24:22	4/1	400	95/138	955/985	291	9476	32
2002 Jan 5	2280.3670/2280.3825	20:48:26/21:10:49	4/1	400	124/127	941/952	242	6637	27
2002 Jan 6	2280.5197/2280.5353	00:28:25/00:50:48	4/1	400	101/112	716/919	200	5871	29
2002 Jan 6	2281.2897/2281.3053	18:57:12/19:19:34	4/1	400	136/142	936/950	230	7065	30
2002 Jan 6	2281.3785/2281.3941	21:05:00/21:27:29	4/1	400	138/144	873/937	200	5043	25
2002 Jan 7	2281.5005/2281.5161	00:00:44/00:23:07	4/1	400	137/146	773/811	252	7473	29

far from being, as they ideally should be, a snapshot of the surface of HR 1099. In this respect, they are susceptible to being affected by long-term changes occurring during the data collection.

Some of the temporal changes in the photospheric distribution can be dealt with by the imaging procedure as long as they can be accurately modelled. This can be done for instance in the case of large-scale surface flows, for which the time dependence of surface motion follows simple laws. For instance, differential rotation is implemented within the imaging code, assuming a rotation law of the form:

$$\Omega(l) = \Omega_{eq} - d\Omega \sin^2 l \quad (1)$$

where $\Omega(l)$ is the rotation rate at latitude l, Ω_{eq} the rotation rate of the equator and $d\Omega$ the difference in rotation rate between the pole and the equator. Section 4 reports our attempt at using this technique to derive differential rotation at the surface of HR 1099 from the present data set. All the images described hereafter are reconstructed

Table 5. Orbital parameters of HR 1099 estimated from our data sets. K_s, γ and ϕ_0 are respectively the radial velocity amplitude of the secondary star, the radial velocity shift of the system and the first conjunction phase of the system. Error bars are of order 0.3 km s^{-1} for K_s and γ, and 2×10^{-4} for ϕ_0.

Epoch	K_s km s^{-1}	γ km s^{-1}	ϕ_0
1998.14	62.80	−14.2	−0.0452
1998.93	62.32	−13.8	−0.0513
1999.06	62.66	−14.5	−0.0541
2000.14	62.85	−14.2	−0.0615
2001.96	62.82	−14.6	−0.0791

Table 6. Characteristics of the reconstructed images. The first and second columns list the epoch and time-span of the data sets. The third and fifth columns respectively list the reduced χ^2 associated to the brightness and magnetic images, while the fourth and sixth columns represent the percentage of spot and the field strength integrated over the stellar surface.

Epoch	Number of nights	χ^2_r Stokes I	Spot (per cent)	χ^2_r Stokes V	B_{int} (G)
1998.14	30	1.2	8.2	1.0	118
1998.93	4	1.1	4.6	0.9	38
1999.06	19	1.2	7.4	0.9	73
1998.93 and 1999.06	58	2.0	4.1	1.0	79
2000.14	35	1.4	8.1	1.2	75
2001.96	37	1.4	6.7	1.3	113

assuming $\Omega_{eq} = 2.222$ rad d^{-1} and $d\Omega = 17$ mrad d^{-1}, following the preliminary estimate of Petit et al. (2001).[1]

More problematic are the local (and unpredictable) modifications of surface structures, such as appearing or vanishing features. This kind of short-term evolution will be discussed in Section 3.3 by comparing our images with those reconstructed from AAT data sets secured typically a few weeks apart from our observations.

The first indication of the temporal variability of surface structures on HR 1099 during the observations comes from the monitoring of the reduced χ^2 (hereafter χ^2_r) of the reconstructed profiles (see Table 6). The χ^2_r of magnetic images ranges from 0.9 to 1.3, while brightness images are reconstructed with a χ^2_r ranging from 1.1 to 1.4 (leaving out the particular case of the images obtained by grouping data obtained at epochs 1998.93 and 1999.06). Splitting large data sets into smaller subsets does not provide a significantly better fit to the data. We thus conclude that on a time-scale of one month, the images are generally not strongly affected by surface variability. However, χ^2_r from Stokes I profiles show a dependence with the length of the data set. The smallest χ^2_r is obtained at epoch 1998.93 (covering four nights only), and the highest one corresponds to epoch 2001.96 (covering as many as 37 nights). Grouping data from the data sets of epochs 1998.93 and 1999.06 yields a χ^2_r of 1.0 and 2.0 for the magnetic and brightness images, respectively, i.e. 11 per cent and 74 per cent above the χ^2_r one can reach when separating both epochs (the better stability of the magnetic χ^2_r can be attributed to the weaker constraint provided by polarized profiles).

[1] Where the differential rotation parameters were by mistake given in rad s^{-1}, instead of rad d^{-1}.

Moreover, the two Stokes I profiles plotted in Fig. 1, taken at rotation phases as close as 0.11 per cent of a rotation cycle, but observed 20 stellar rotations apart, show clear differences (reaching as much as 9 per cent of the line depth) between both observations (while all profiles obtained around phase 0.71 are very similar in shape, see Fig. 2). The blue part of the latest profile shows a bump corresponding to a new-born spot located at phase 0.8 and latitude 40° (Fig. 3), while the red wing of the profile is deeper, owing to the disappearance of the polar spot appendage pointing toward phase 0.55 in the 1998.93 image. These differences demonstrate that surface variability can no longer be ignored on a time-scale of order 2 months.

3.2 Long-lived surface structures

The magnetic images of HR 1099 reported in Figs 2, 3, 4, 5 and 6 show most of the characteristics already outlined by Donati et al. (1992), Donati (1999) and D03a.

The most obvious surface feature in the brightness images is the large, high-contrast polar spot appearing in all reconstructed images. This feature is never centred on the pole, but is usually concentrated higher than latitude 60°. Its shape can be rather complex, for instance at epoch 1998.14, when its main component was located at phase 0.55 and latitude 60°, with several satellite spots forming a partial ring around the pole. Apart from the high-latitude spot, several smaller spots or groups of spots (as in Fig. 6) appear at lower latitude (close to the equator) on all images. Cross-correlating all latitude rings of brightness images obtained at different epochs does not show evidence of any particular longitudinal dependence of the low-latitude structure occupancy.

Some magnetic features we discuss hereafter have been repeatedly observed over 13 years since the first images of Donati et al. (1992). These structures, detected through several instrumental set-ups, are also consistently reproduced with different inversion techniques (see the magnetic image of HR 1099 obtained with spherical harmonic decomposition from the Stokes V data set of epoch 1998.14 presented here, assuming either an unconstrained or a linear combination of force-free fields, Donati 2001).

In particular, we note the persistent presence of magnetic regions in which the field is mostly horizontal (i.e. parallel to the surface). These regions show up as two distinct azimuthal field regions of opposite polarity. The first of these regions is a ring of counter-clockwise field confined at a latitude of about 30°. This ring appears fragmented in all images (partly due to the effect of incomplete phase coverage in the case of magnetic topologies associated with epochs 1998.93 and 1999.06). The latitude of the ring does not evolve between 1998.14 and 2001.96. We also note that the ring is never perfectly axisymmetric, but rather appears as a string of spots of intense magnetic field.

The second region with horizontal field is a ring of clockwise azimuthal field above latitude 60°. At two epochs (2000.14 and 2001.96), the ring draws a well-defined circle centred on the pole, with a field intensity in excess of 1 kG. On the other images, this magnetic region is reconstructed as a bipolar pair centred on the pole, both in the azimuthal and meridional components of the field. As explained by Donati (1999), such bipolar pairs are only a visual artefact produced by the projection of the field in spherical coordinates, reflecting a single magnetic structure of horizontal and roughly homogeneously oriented field, passing through the pole. On our images, the centre of the ring is steadily located between phases 0.5 and 0.6.

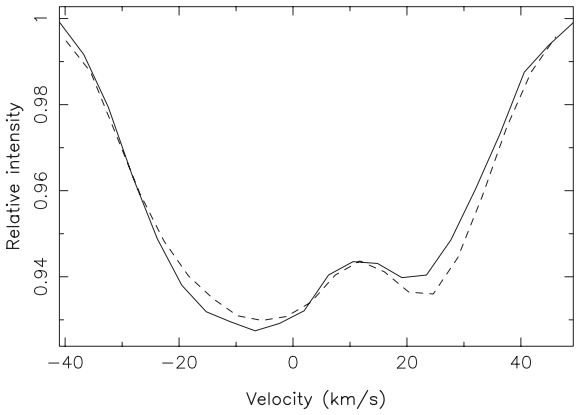

Figure 1. Mean Stokes I profiles obtained at phase 0.7125 on 1998 December 05 (full line) and phase 0.7136 on 1999 January 31 (dashes). The difference between both observations reaches 9 per cent of the line depth.

The other magnetic regions are mainly radial field spots. Their distribution is more complex than the horizontal field regions and shows weaker correlation from one epoch to the next. Global trends in their distribution over the stellar photosphere can be distinguished, though. If we consider the longitudinally averaged radial and azimuthal components of the algebraic magnetic field as a function of latitude (i.e. their contribution to the axisymmetric component of the large-scale field, Fig. 7), we clearly observe a predominance of positive radial field above latitude 60°, most spots of negative polarity being confined at lower latitudes. Moreover, the latitude limit between these two regions roughly corresponds to the transition region between both rings of azimuthal magnetic field. These conclusions are fully consistent with those of D03a. We also confirm that the axisymmetric component of the magnetic topology is very stable over years, as can be deduced from comparison of Fig. 7 with a similar plot in Donati (1999).

3.3 Short-term evolution of surface structures

The time interval between TBL and AAT observations never exceeds two months. The comparison of the two data sets gives us the first opportunity for studying in detail the short-term evolution of the structures at the surface of HR 1099.

First of all, the observations at epoch 2001.96 (2001.99 at the AAT) represent the first bi-site simultaneous spectropolarimetric observations of HR 1099. Comparing the resulting images constitutes the most accurate consistency check one can perform. The main difference between both data sets is the shorter time-span of AAT observations (covering about one-third of the observing time spent at TBL at the same epoch). We first note that all large magnetic and brightness structures, i.e. the rings of horizontal field, the radial field regions and the high-latitude starspots, all feature a location, shape and intensity that agree very well in both images. Of particular interest is that the similarity still holds for low-latitude structures as well, demonstrating that reconstruction biases (usually stronger at such latitudes) are essentially insignificant in our case.

On the other hand, brightness images show at least one clear discrepancy for one spot located at latitude 20° and phase 0.40. This spot, appearing as a large and contrasted feature in the TBL image, shows up only as a weak blob in the AAT image. An image (not shown here) reconstructed from a subset of our data selecting only spectra secured within the AAT observing window confirm that these differences are actually due to photospheric variability acting within less than two weeks. Differences are also visible in the details of the polar spot, suggesting that small structures may have a lifetime of order only a few weeks.

The same kind of evolution is detected at other epochs as well, with similarity between AAT and TBL images decreasing for an increasing time-gap between observations. The comparisons are, however, limited by the difference in phase coverage between TBL and AAT images, which restrict such considerations to high-latitude features, or to regions well-monitored with both instruments.

To the relatively short lifetime of the smallest structures in the brightness and radial field images, we can contrast the longer-term stability of larger patterns. In fact, the only striking example of a large-scale reorganization of the photospheric magnetic field within a short time is visible at epoch 2000.14, where the large, intense azimuthal field spot located at phase 0.57 in the 1999.97 AAT image seems to have almost completely vanished from the TBL image, obtained two months later. Another such difference is that the overall field strength inside the low-latitude azimuthal field ring is significantly smaller at epoch 2001.96 than at 2001.99.

3.4 Long-term evolution of surface structures

As already emphasized, the axisymmetric component of the field topology is remarkably stable over years. No change as obvious as a global polarity switch has yet been observed in the succession of images presented in this study, nor in any other similar studies (Donati 1999 D03a). In particular, the latitudinal location of the rings of azimuthal magnetic field does not significantly evolve from one epoch to the next. However, our observations confirm the trend pointed out by D03a, who reported that the relative fraction of the magnetic energy contained inside the horizontal component of the field was fluctuating with time. From our observations (assuming that the meridional field should be counted as part of the radial component for latitudes less than 45°, owing to the cross-talk problem mentioned in Section 2.2), we derive a fraction equal to 79 and 56 per cent at epochs 1998.14 and 2000.14, respectively (77 per cent when averaged over all observing epochs), thus showing that the toroidal component of the field usually contains most of the magnetic energy, except at epoch 2000.14, when both components were of equal importance.

From cross-correlating the latitude rings between brightness images obtained at different epochs (assuming a solid-body rotation of the stellar surface with a rotation period of 2.83774 d), we observe a regular angular shift of the high-latitude spot toward increasing phases. This trend is also readily visible on the brightness images themselves, as well as on those of D03a. It is also compatible with previous images (Donati 1999) except for that corresponding to epoch 1991.96. This regular phase shift of the polar spot is associated with a beat period of about 10–12 yr. This apparent rotation of persistent polar features can also be tracked from the high-latitude radial field features. However, we must keep in mind that the presence of the very dark brightness polar region is likely to influence the location of the reconstructed magnetic field at high latitude, therefore introducing a potential spurious correlation between the locations of brightness and radial field structures close to the pole.

4 DIFFERENTIAL ROTATION

4.1 Principle

Owing to the rotation period of HR 1099 (very close to the orbital period of 2.83774 d), single-site observations of this star cannot provide data sets with dense phase sampling over one single rotation cycle. At the latitude of Pic du Midi for instance, observations of HR

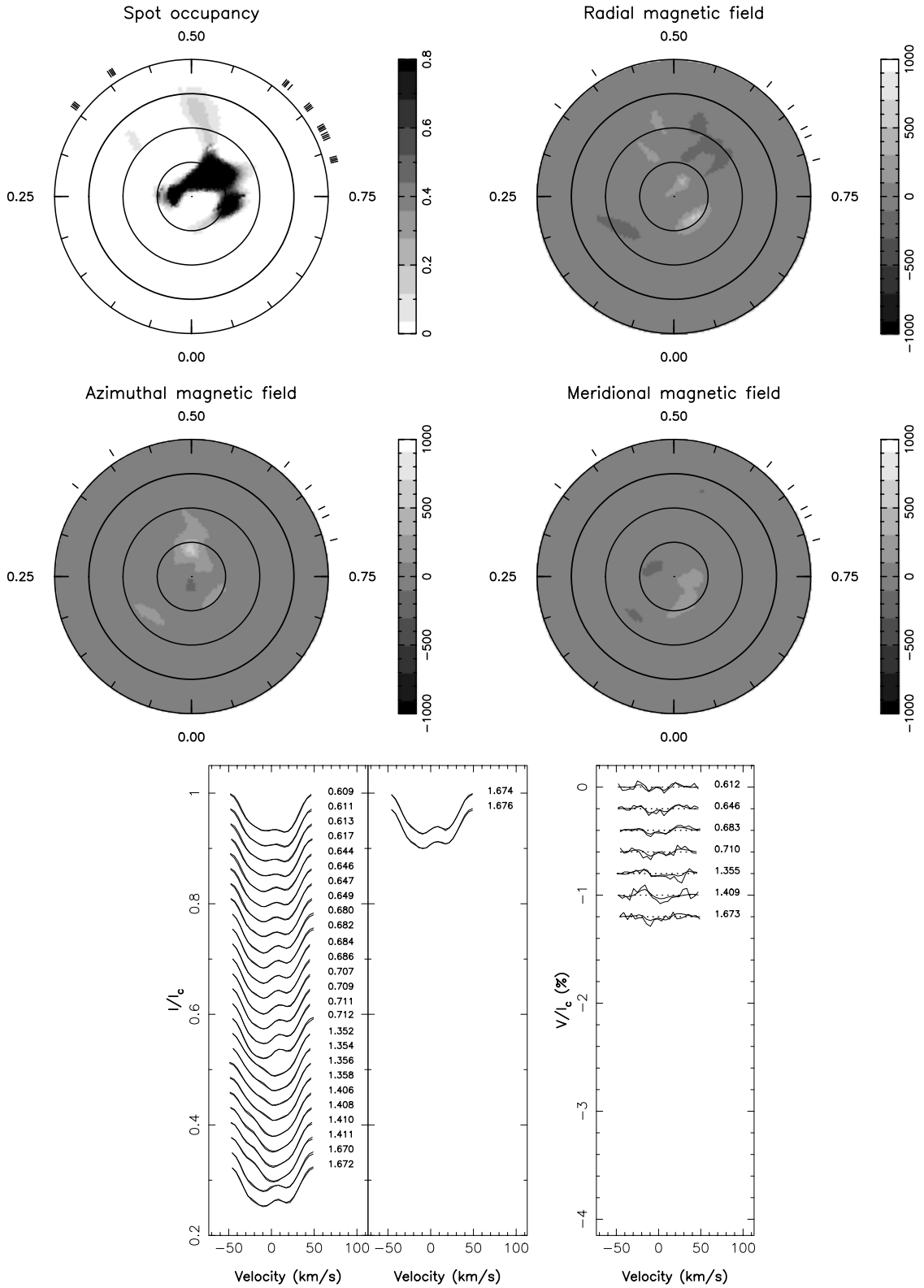

Figure 2. Reconstructed images of the primary star of HR 1099 at epoch 1998.93, in flattened polar view. The concentric circles correspond (from outer side to centre) to parallels of latitude -30°, 0° (equator, bold line), $+30^\circ$ and $+60^\circ$. The upper-left panel corresponds to a brightness image, while the three other panels show the components of the magnetic field (in gauss) in spherical coordinates, i.e. radial, azimuthal and meridional components of the field in the upper-right, lower-left and lower-right panels, respectively. Mean Stokes I and V profiles (left-hand panel and right-hand panel, respectively) of the primary star of HR 1099 for the 1998.14 data set are also depicted in the bottom graph. Thin lines represent the observed profiles, while bold lines correspond to the profiles reconstructed by the imaging code.

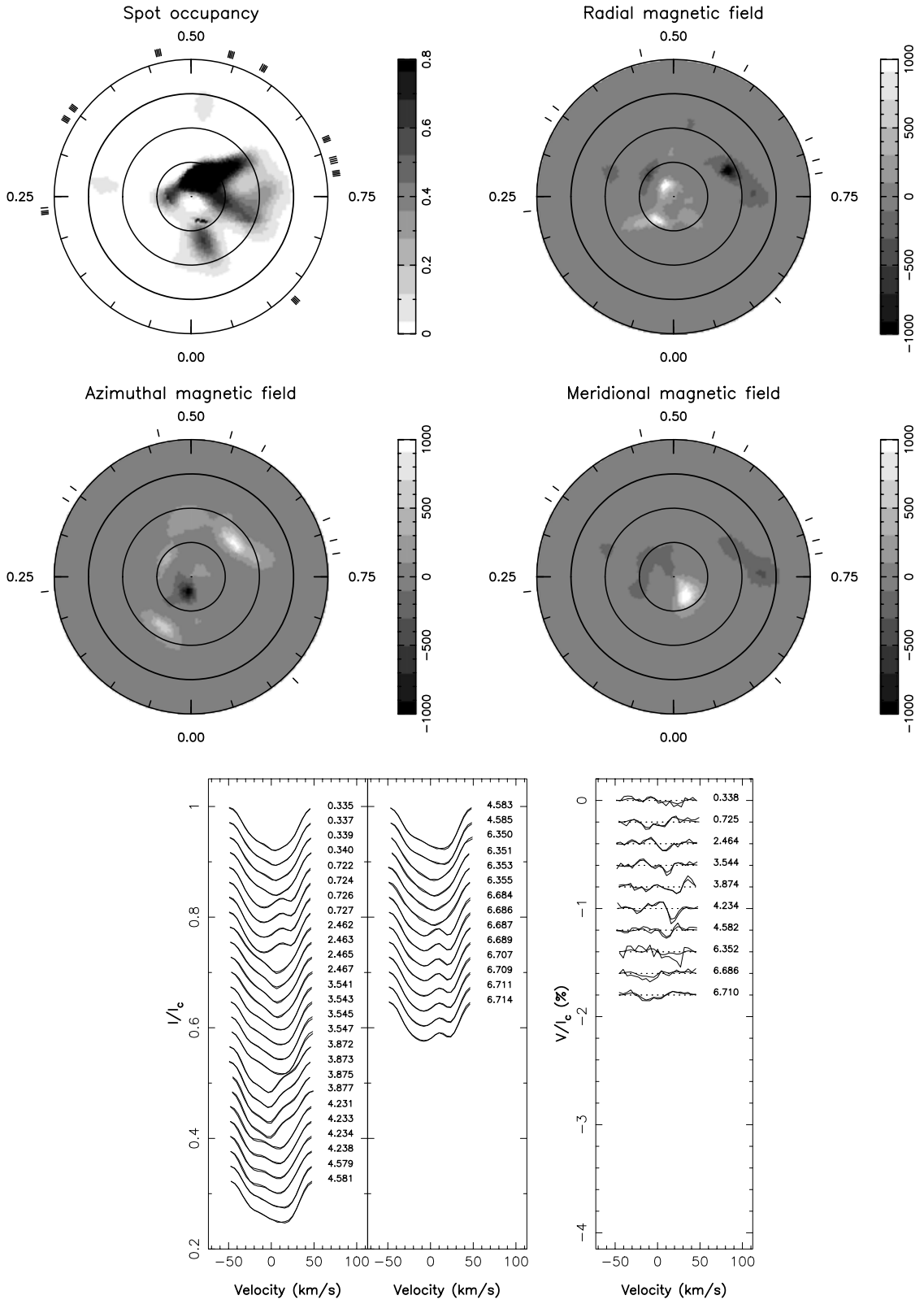

Figure 3. Same as Fig. 2 for the 1999.06 data set.

1099 can hardly cover more than 15 per cent of a rotation cycle per night, with almost redundant phase observation every 3 d, except for a small shift of 5.7 per cent of a rotation cycle. A very dense phase sampling of HR 1099 thus requires 18 d in theory, and often more than one month in practice. It implies at the same time that our images of HR 1099 cannot be considered as snapshots and that any kind of temporal variability (like large-scale surface flows) are likely to distort the surface patterns during data collection. In this section,

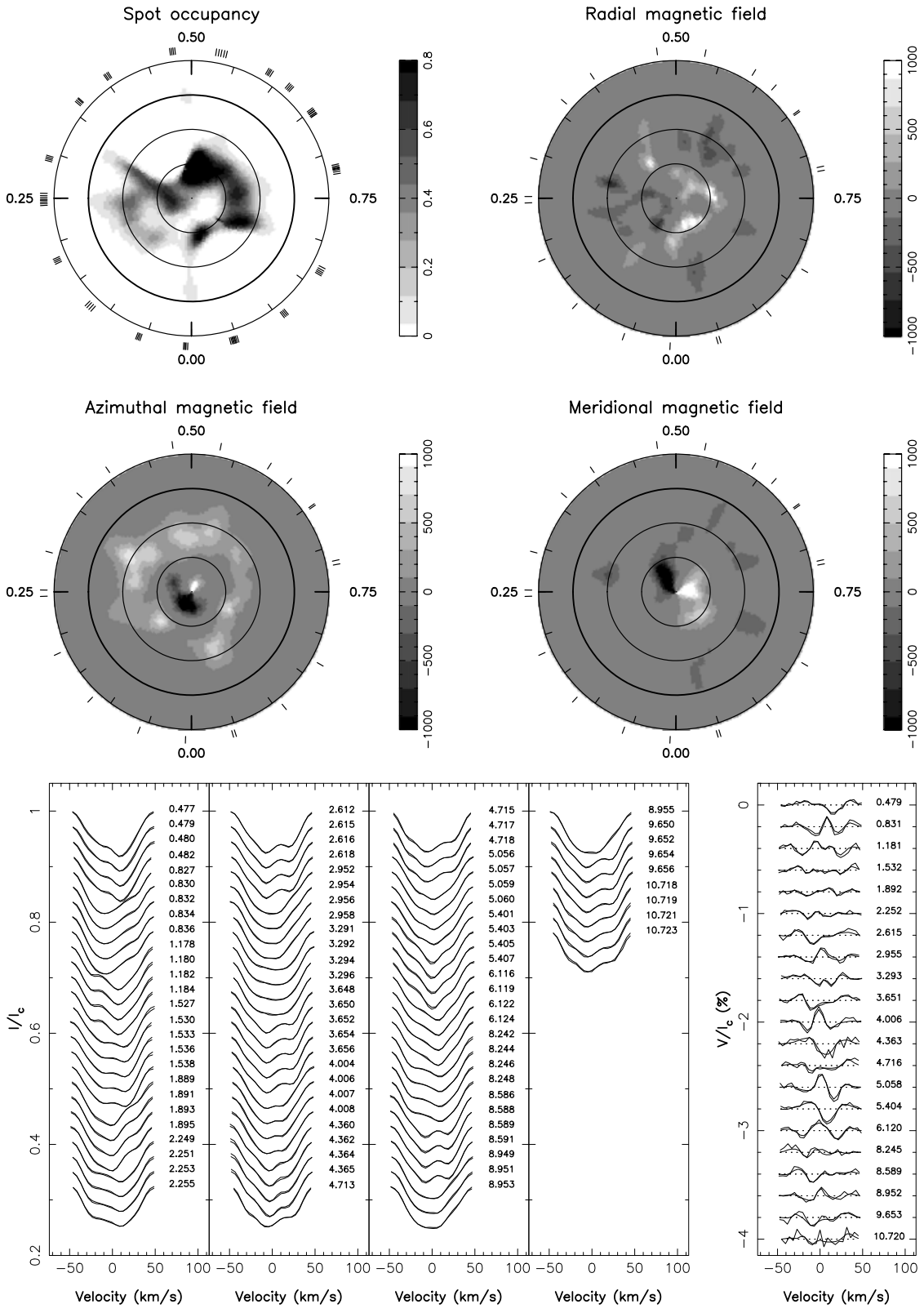

Figure 4. Same as Fig. 2 for the 1998.14 data set.

we present an estimate of the photospheric shear at the surface of HR 1099 induced by differential rotation.

First of all, we note that the restrictive observing conditions inherent to HR 1099 make inappropriate the techniques commonly used for estimating the surface rotational shear, based on cross-correlating two successive images of the star. As mentioned in Section 3.3, images obtained at distant epochs are not correlated, except for the location of the permanent polar spot. No information about

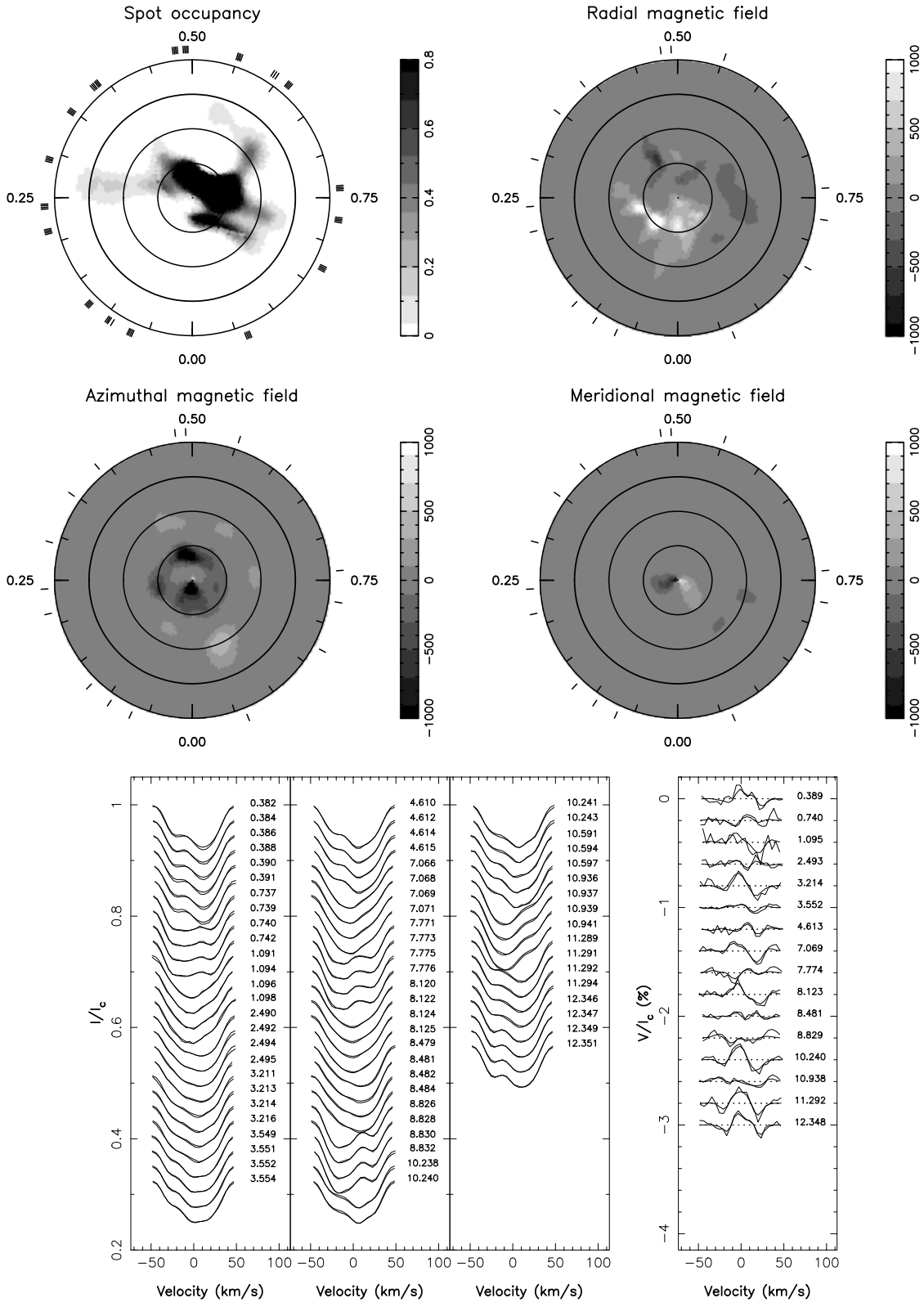

Figure 5. Same as Fig. 2 for the 2000.14 data set.

differential rotation can thus be extracted from such image comparison. The second possibility would be to split our data sets into smaller subsets and compare the successive images obtained from each subset. However, as pointed out by Petit et al. (2002), the induced reconstruction biases are in this case likely to dominate the differential rotation signal.

We therefore choose the dedicated method of Petit et al. (2002), which proves to be well-adapted to the case of intermediate rotators

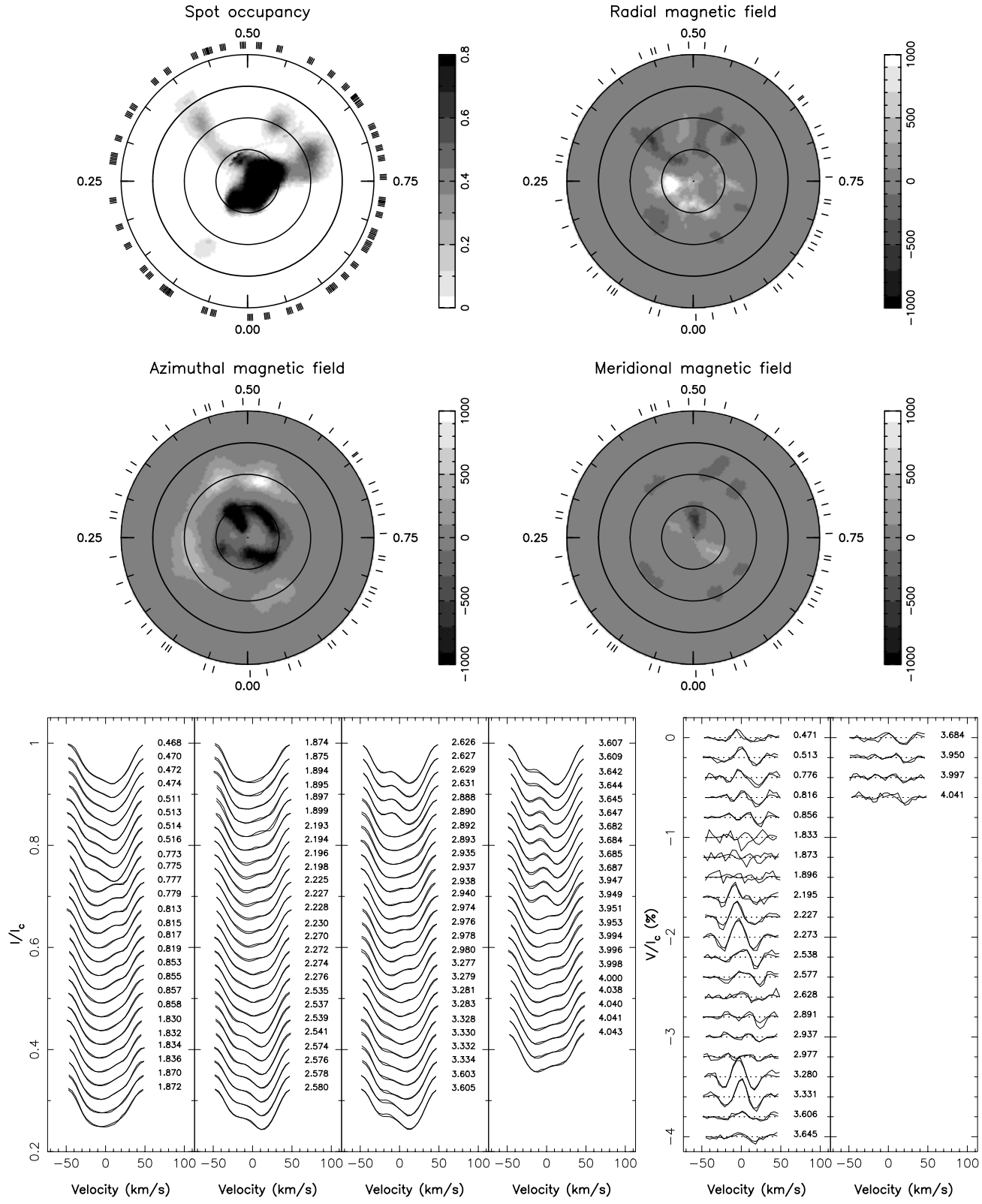

Figure 6. Same as Fig. 2 for the 2001.96 data set.

like HR 1099. This method is based on the reconstruction of brightness and magnetic images for various sets of differential rotation parameters (Ω_{eq} and dΩ, see equation 1) in order to find the parameter pairs that minimize the information content of the reconstructed images.

4.2 Differential rotation measurements

The differential rotation parameters derived from our sets of brightness and magnetic profiles are listed in Table 7 and shown in Fig. 8. We first note that a rotational shear (evaluated by the dΩ parameter)

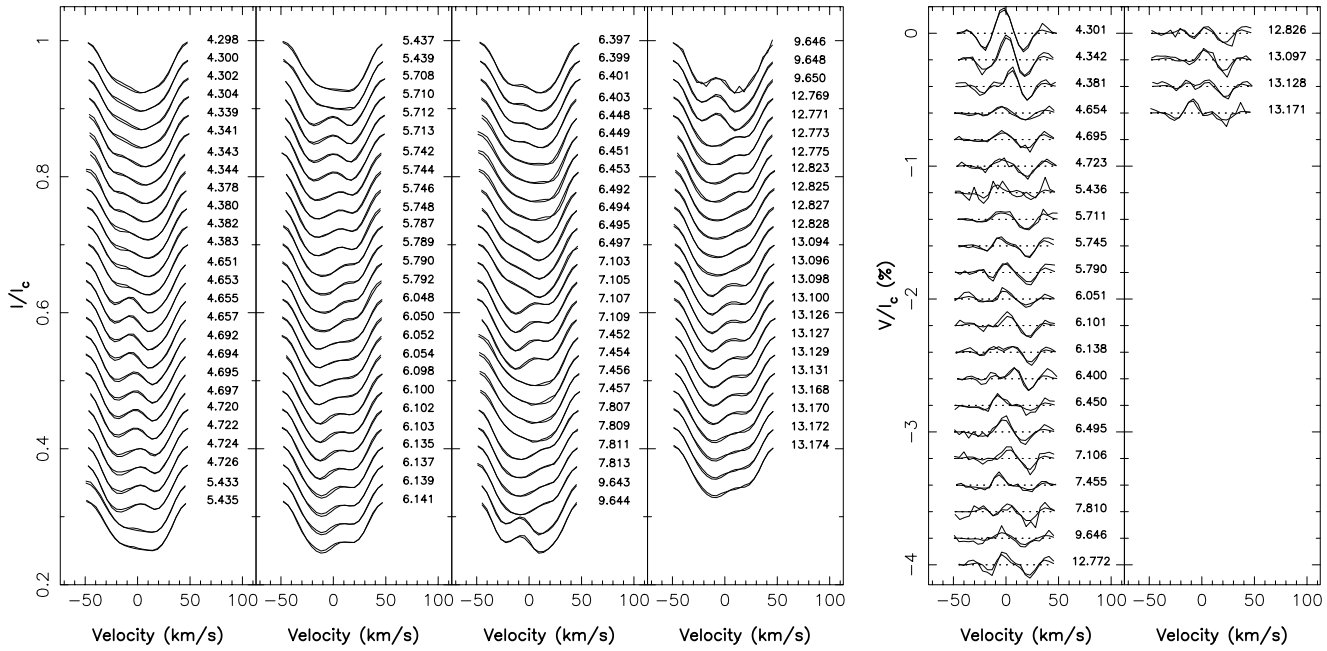

Figure 6. (*Continued*).

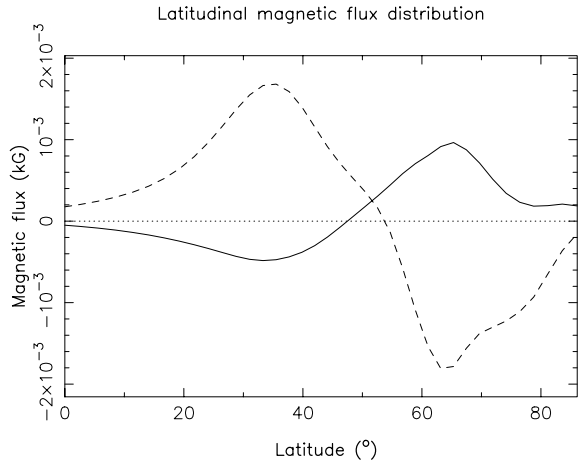

Figure 7. Latitudinal distribution of the radial (full line) and azimuthal (dashed line) components of the magnetic field, averaged over all observing epochs.

is firmly detected in our Stokes I data sets (to within as much as 7σ at epoch 2001.96) as well as in our Stokes V data sets (to within 4σ at epochs 1998.14 and 2001.96). The parameters derived from some epochs are less accurate, and several data sets did not provide any reliable estimates, with error bars greater than a few tens of mrad d^{-1}. Not surprisingly, the most accurate sets of profiles are those collected on the largest time-span, therefore displaying the largest shifts of surface structures during data collection. A high quality level of the data is also necessary, as can be illustrated by the poor result derived from the Stokes I profiles of epoch 2000.14, mostly reflecting the rather low S/N of this data set.

However, expanding the time-span above the lifetime of photospheric structures increases the risk of obtaining spurious differential rotation detection, produced by aliases between tracers appearing at close-by locations at the stellar surface. This effect is already present when grouping 1998.93 and 1999.06 Stokes I profiles. The newly born low-latitude spot group located around phase 0.75 at epoch 1999.06 (Fig. 3) can indeed be mistaken for the disappearing spot visible at phase 0.5 at epoch 1998.93 (Fig. 2), erroneously suggesting a strongly antisolar differential rotation (i.e. with the stellar equator rotating slower than the pole). This obviously spurious solution is indeed suggested by our measurements as a secondary χ^2_r minimum, in addition to the differential rotation parameters reported in Table 7 (and equal to 2.1934 ± 0.0059 rad d^{-1} and -24.6 ± 8.8 mrad d^{-1} for Ω_{eq} and $d\Omega$ respectively). This effect, which can obviously be tracked down in the data themselves in this particular case, can occur in a much more subtle way in other situations, and generate systematic biases of the reconstructed differential rotation parameters. This example tells us that we cannot derive reliable parameters from data sets collected on a time-scale longer than the lifetime of the small surface structures, i.e. typically four weeks.

Most observations secured at the AAT are not close enough to our own observations to guarantee that surface variability will not degrade the surface differential rotation estimates. The only epoch for which AAT and TBL data can be safely grouped is the bi-site campaign of 2001.96 (TBL) and 2001.99 (AAT). The extremely dense data set thus generated (308 Stokes I profiles and 77 Stokes V profiles altogether) constitutes an excellent base to derive a differential rotation law, with both an optimal time-span of 37 nights and a high S/N. The resulting set of parameters is consistent with independent estimates derived from TBL and AAT subsets alone, providing the most accurate estimate of a surface shear ever achieved on a fast rotator, with an uncertainty on $d\Omega$ of the order of 1 mrad d^{-1} only.

Finally, we note that the differential rotation parameters we derive do not show evidence for strong time-variability, as reported by, e.g. D03b on younger objects. We speculate that this essentially results from the large relative error bars of our estimates. Only one of the estimates (corresponding to the 1998.14 Stokes V data) significantly differs from the other values (see Fig. 8), with a 2.75σ discrepancy

Table 7. Surface rotation parameters derived from HR 1099 TBL observations. For each epoch, Ω_{eq} (equatorial rotation rate) and dΩ (difference of rotation rate between equator and pole) are listed for the reconstructed brightness profiles (columns 2 and 3) and for the associated Stokes V profiles (columns 4 and 5). Line 4 gives the parameters derived from a data set obtained by grouping 1998.93 and 1999.06 profiles sets, and the last line provides the differential rotation law derived when grouping the 2001.96 data set obtained at the TBL with the 2001.99 observations secured by D03a at the AAT.

Date	Brightness images		Magnetic images	
	Ω_{eq}	dΩ	Ω_{eq}	dΩ
year	rad d^{-1}	mrad d^{-1}	rad d^{-1}	mrad d^{-1}
1998.14	2.22018 ± 0.0018	10.6 ± 3.1	$2.2464 \pm .0059$	40.9 ± 9.2
1998.93	2.209 ± 0.033	15.6 ± 39.8	–	–
1999.06	2.2241 ± 0.0045	21.8 ± 9.2	2.219 ± 0.011	18.9 ± 25.6
1998.93 and 1999.06	2.2172 ± 0.0029	10.6 ± 4.4	2.2201 ± 0.0032	24.1 ± 6.4
2000.14	2.1915 ± 0.0096	-3.8 ± 14.3	2.233 ± 0.011	28.6 ± 17.2
2001.96	2.2206 ± 0.0009	13.2 ± 1.7	2.2269 ± 0.0023	17.0 ± 3.8
2001.96 and 2001.99	2.2241 ± 0.0004	15.21 ± 0.82	2.2232 ± 0.0009	9.68 ± 1.8

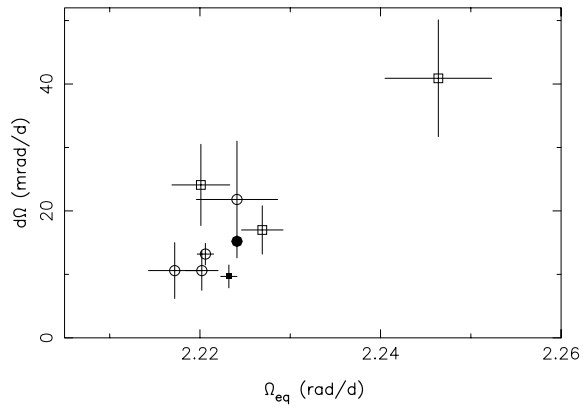

Figure 8. Estimates of differential rotation parameters obtained with TBL data sets. The circles (respectively squares) represent estimates derived from Stokes I (respectively Stokes V) profiles. The plotted data points are only those with error bars smaller than 10 mrad d^{-1}. The black-filled symbols represent the parameters obtained when grouping 2001.96 and 2001.99 data sets (i.e. TBL and AAT observations). Note that the error bar corresponding to the Stokes I profiles of epoch 2001.96 and 2001.99 is smaller than the symbol width.

for Ω_{eq}, but with dΩ consistent with other measurements. Further estimates with smaller error bars are needed to confirm that such a variability can indeed arise from a physical process.

5 DISCUSSION

We report evidence that the surface of the primary star in HR 1099 is differentially rotating, with a lap time (time for the equator to lap the pole by one complete cycle) of the order of 480 d. This result does not confirm previous studies of Vogt et al. (1999) and Strassmeier & Bartus (2000), reporting that the differential rotation of HR 1099 is antisolar, i.e. with its pole rotating faster than its equator. We emphasize, however, that such studies were carried out with low S/N and sparse phase sampling. Moreover, we insist on the fact that the result presented here is repeatedly derived from completely independent data sets obtained at different epochs (from 1998.14 to 2001.96), with different instruments (MuSiCoS and UCLES), and consistently recovered both from brightness and magnetic images. Moreover, the difference of rotation rate between the pole and the equator we derive in the present work (d$\Omega = 15.2 \pm 0.8$ mrad d^{-1}) is in agreement with the period variations observed in photometric studies (d$\Omega = 13.1$ mrad d^{-1}, Henry et al. 1995).

The most intriguing result of our study is that the rotational shear we measure is significantly weaker than those previously estimated on other active fast rotators (Donati & Cameron 1997; Donati et al. 2000; Barnes et al. 2000, who measured lap times 4–12 times shorter than in the present study). Moreover, the lap time of the primary star in HR 1099 is four times smaller than that of the Sun. The first reason we may invoke to explain this discrepancy is the evolutionary stage of the primary component (a subgiant) of HR 1099. As reported in a companion paper (Petit et al. 2004), the differential rotation on the G5 FK Com (sub)giant HD 199178 is again of the same magnitude as that of the Sun (i.e. about four times stronger than that of HR 1099), despite its similarly deep convective zone. Sadly enough, HD 199178 cannot be taken as a strict analogue to HR 1099, for example because of its higher mass (1.65 $M_{\odot}$). Such a difference may indeed partly explain its stronger surface shear, as suggested by other observational studies (Donati et al. 2000; Reiners & Schmitt 2002). However, this dependence of differential rotation on stellar mass was detected on young dwarfs, and may not hold for more evolved objects with very deep convective zones. The effect that may most likely weaken the surface shear of HR 1099 is the strong tidal forces that it suffers, imposing very efficiently corotation, not only to the binary system itself, but also to the rotation within the convective zones of both stars. A possible consequence of these tidal forces is to limit the amount of the surface shear. The theoretical work of Scharlemann (1981, 1982) shows that the differential rotation of an evolved component of a RS CVn system is indeed likely to be strongly weakened (though not totally suppressed), in very good agreement with our observations. In the case where the shear persists, the stellar envelope is still forced to corotate on average, which means that part of the envelope rotates faster than the system, the other part slower, and that there is a corotating latitude. In our case, this latitude of corotation is equal to 50°.

Applegate (1992) predicts that the fluctuations of the orbital period of the system (monitored as the conjunction phase ϕ_0) may be related to an exchange between kinetic and magnetic energy of the convective zone during the magnetic cycle, and may also show up as temporal variations of the differential rotation. Owing to the fact that small error bars were only achieved from the bi-site campaign of 2001.96 and 2001.99, we have not yet detected definite variations of the parameters, and are not yet able to confirm or contradict this prediction. However, the expected dΩ fluctuations required by this mechanism (from d$\Omega \approx 0$ to d$\Omega \approx 40$ mrad d^{-1}, D03b) are still

roughly compatible with our results and make this issue a promising prospect for future observations.

As reported by D03b, the angular momentum J within a stellar convective zone may be simply related to the rotation parameters measured at the surface of the star in the case of simple models of the velocity field within the convective envelope:

$$J(\Omega_{\rm eq}, {\rm d}\Omega) \propto \Omega_{\rm eq} - \lambda\, {\rm d}\Omega \quad (2)$$

where λ depends on the assumed internal rotation model and on the internal stellar structure. In the particular case where the velocity field is supposed to be close to that of the Sun (angular rotation rate not depending on the distance from the centre of the star), λ is equal to 0.2. For the velocity fields expected for very rapid rotators (angular rotation constant over axisymmetric cylinders), λ becomes dependent on stellar internal structure, and is equal to 0.68 in the case of HR 1099 (D03b). In the case of HR 1099, one can safely consider that tidal forces are strong enough to impose average corotation within the convective zone. This means in particular that $\Omega_{\rm eq}$ will be equal to the orbital rotation rate $\Omega_0 = 2,21415$ rad d^{-1} whenever differential rotation is suppressed within the convective zone, i.e. that $J(\Omega_{\rm eq}, {\rm d}\Omega) = J(\Omega_0, 0)$. Using the most accurate values of $\Omega_{\rm eq}$ and dΩ we have estimated (from the Stokes I and V data sets secured at epoch 2001.96 and 2001.99), the values of λ we derive from this relation are equal to 0.7 ± 0.1 and 0.9 ± 0.2 for Stokes I and V data, respectively. This result suggests that the angular velocity field inside the deep convective envelope of HR 1099 is close to that expected for rapid rotators.

The weakness of the surface differential rotation of HR 1099 is of course a major constraint when investigating the dynamo processes generating its magnetic topology. The most interesting feature of the reconstructed topology is the presence of a strong azimuthal component of the magnetic field at the surface of the star, which may be related to the large-scale toroidal component of the dynamo field. In the case of the Sun, the large-scale toroidal field is believed to be confined at the interface layer between the radiative core and the convective envelope. The fact that it reaches the photospheric level may therefore suggest (as was already pointed out in several articles, see e.g. D03a) that the dynamo may be partly distributed in the convective envelope, or at least significantly active close to the surface. Moreover, the regions of azimuthal field are close to axisymmetry (at least when averaged on several years). This behaviour is more obvious on HR 1099 than on any object of the sample of young active stars for which magnetic topologies have been reconstructed up to now. As mentioned by D03a, the deep convective zone of the primary in HR 1099 allows the maintenance of a strong dynamo activity despite the rather low differential rotation. In any case, the detection of a well-structured surface azimuthal field (along with a definite differential rotation) suggests that an $\alpha\Omega$ dynamo is operating in this star, implying that the numerical simulations of dynamo processes in tidally interacting stars carried out by Moss & Tuominen (1997) (assuming that there is no differential rotation in the stellar convective zone and that only α^2-type dynamos can be generated) may not apply here.

Our study of short-term and long-term variability of HR 1099 shows that surface changes are significant for the smallest structures on a time-scale of only a few weeks. This typical evolution time holds both for brightness and magnetic spots. Such a variability clearly shows that differential rotation measurements reported by Vogt et al. (1999) (based on comparison of images secured several months apart) are likely to suffer from the aliasing problems that we tried to avoid in the present study. The largest axisymmetric structures (the large polar spot and the rings of azimuthal magnetic field) show a much longer-term stability (longer than a decade). The long lifetime of most surface structures on HR 1099 (longer than for AB Dor, Donati & Cameron 1997) may be related to the smaller surface shear of HR 1099.

Finally, we note that the present observations of the magnetic topology of the primary star in HR 1099 do not indicate major changes in the magnetic topology of this star during the last 10 years. In particular we do not detect, as on LQ Hya (Donati 1999, D03a), any trend announcing a global polarity switch of the magnetic patterns. However, we confirm the discovery of D03a who pointed out that the relative weights of the poloidal and toroidal components of the field are varying with time. The toroidal component of the field in HR 1099 always dominates the magnetic flux, except at epoch 2000.14, when the large-scale toroidal and poloidal fields contained the same level of energy. The monitoring of such fluctuations may provide some important tests for future stellar dynamo theories.

6 CONCLUSIONS AND PROSPECTIVES

This study, showing evidence for a weak solar-like differential rotation at the surface of the primary K1 subgiant of the RS CVn system HR 1099 (with a lap time of order 480 d), gives preliminary indications of the impact of tidal forces on the convective zones of late-type components of close binary systems.

However, we critically lack differential rotation measurements on a sample of single evolved fast rotators to prove that such a weak surface shear is indeed due to a tidal torque, rather than to other stellar parameters, such as the depth of the convective zone or the stellar mass. We have already started this systematic investigation with the study of the FK Com G5 (sub)giant HD 199178 (Petit et al. 2004), and we will soon pursue our investigations with FK Com itself. We are also carrying out the same type of study on other RS CVn systems (UX Ari, II Peg, σ Gem) in order to investigate if a weak surface differential rotation is a general feature of close late-type binaries.

Finally, we plan to pursue our monitoring of the above-mentioned active stars with the new generation spectropolarimeters (ESPaDOnS at the CFHT and NARVAL at the TBL), to benefit from increased spectral resolution and S/N, and from the opportunity to conduct the multisite studies that prove to be necessary to obtain accurate estimates of differential rotation in intermediate rotators. Such high-quality data, along with long-term monitoring engaged with the present article, should make it possible to test Applegate's (1992) prediction that differential rotation of RS CVn systems may vary during a magnetic cycle, and may be connected with the observed fluctuations of the orbital periods of these objects.

ACKNOWLEDGMENTS

GAW, JDL, SLSS, SS and TAAS acknowledge grant support from the Natural Sciences and Engineering Research Council of Canada (NSERC).

REFERENCES

Applegate J. H., 1992, ApJ, 385, 621
Barnes J. R., Cameron A. C., James D. J., Donati J.-F., 2000, MNRAS, 314, 162
Baudrand J., Böhm T., 1992, A&A, 259, 711
Brown S. F., Donati J.-F., Rees D. E., Semel M., 1991, A&A, 250, 463
Cameron A. C., 1992, in Byrne P. B., Mullan D. J., eds, Surface Inhomogeneities on Late-Type Stars. Springer, Berlin, p. 33

Cameron A. C., Donati J.-F., Semel M., 2002, MNRAS, 330, 699
Donati J.-F., 1999, MNRAS, 302, 457
Donati J.-F., 2001, in Boffin H., Steeghs D., Cuypers J., eds, AstroTomography, Indirect Imaging Methods in Observational Astronomy. Springer, Berlin, p. 207
Donati J.-F., Brown S. F., 1997, A&A, 326, 1135
Donati J.-F., Cameron A. C., 1997, MNRAS, 291, 1
Donati J.-F., Brown S. F., Semel M., Rees D. E., Dempsey R. C., Matthews J. M., Henry G. W., Hall D. S., 1992, A&A, 265, 682
Donati J.-F., Semel M., Carter B. D., Rees D. E., Collier Cameron A., 1997, MNRAS, 291, 658
Donati J.-F., Catala C., Wade G. A., Gallou G., Delaigue G., Rabou P., 1999a, A&AS, 134, 149
Donati J.-F., Cameron A. C., Hussain G. A. J., Semel M., 1999b, MNRAS, 302, 437
Donati J.-F., Mengel M., Carter B. D., Cameron A. C., Wichmann R., 2000, MNRAS, 316, 699
Donati J.-F. et al., 2003a, MNRAS, 345, 1145 (D03a)
Donati J.-F., Cameron A. C., Petit P., 2003b, MNRAS, 345, 1187
Henry G. W., Eaton J. A., Hamer J., Hall D. S., 1995, ApJS, 97, 513
Moss D., Tuominen I., 1997, A&A, 321, 151
Petit P. et al., 2001, in Boffin H., Steeghs D., Cuypers J., eds, AstroTomography, Indirect Imaging Methods in Observational Astronomy. Springer, Berlin, p. 232
Petit P., Donati J.-F., Cameron A. C., 2002, MNRAS, 334, 374
Petit P. et al., 2004, MNRAS, submitted
Piskunov N., 2001, in Mathys G., Solanki S. K., Wickramasinghe D. T., eds, ASP Conf. Ser. Vol. 248, Magnetic Fields across the Hertzsprung–Russell Diagram. Astron. Soc. Pac., San Francisco, p. 293
Reiners A., Schmitt J. H. M. M., 2002, A&A, 393, L77
Scharlemann E. T., 1981, ApJ, 246, 292
Scharlemann E. T., 1982, ApJ, 253, 298
Skilling J., Bryan R. K., 1984, MNRAS, 211, 111
Strassmeier K. G., Bartus J., 2000, A&A, 354, 537
Unruh Y. C., Cameron A. C., 1995, MNRAS, 273, 1
Vogt S. S., Hatzes A. P., Misch A. A., Kürster M., 1999, ApJS, 121, 547

This paper has been typeset from a TEX/LATEX file prepared by the author.